Supplementary information

A Hypervalent and Cubically Coordinated Molecular Phase of IF_8 Predicted at High Pressure

Dongbao Luo,[1‡] Jian Lv, [1‡] Feng Peng,[4] Yanchao Wang,[1] Guochun Yang,[2*] Martin Rahm,[3*]and Yanming Ma[1,5*]

1. International Center of Future Science, Jilin University, Changchun 130012, China State Key Laboratory of Superhard Materials, College of Physics, Jilin University, Changchun 130012, China

2. Centre for Advanced Optoelectronic Functional Materials Research and Laboratory for UV Light-Emitting Materials and Technology of Ministry of Education, Northeast Normal University, Changchun 130024, China

3. Department of Chemistry and Chemical Engineering, Chalmers University of Technology, 412 96, Gothenburg, Sweden

4. College of Physics and Electronic Information, Luoyang Normal University, Luoyang 471022, China

5. International Center of Future Science, Jilin University, Changchun 130012, China

*Address correspondence to: yanggc468@nenu.edu.cn; martin.rahm@chalmers.se ; mym@calypso.cn

Index **page**

Computational Details

The structural prediction approach is based on a global minimization of free energy surfaces merging *ab initio* total-energy calculations through CALYPSO (Crystal structure AnaLYsis by Particle Swarm Optimization) methodology as implemented in its same-name CALYPSO code.[1-2] Our structure search for IF_n (n >1) compounds is performed with the formula units (f.u.) up to 4 at 100, 200, and 300 GPa, respectively. In the first generation, a population of structures with certain symmetry are constructed randomly. Local optimizations of the generating structures are done with the conjugate gradients method through the VASP code, with an economy set of input parameters and an enthalpy convergence of 1×10^{-5} eV per cell.[3-4] Step in the second generation, 60% of them with lower enthalpies are selected to produce the next generation structures by PSO, and 40% of the structures in the new generation are randomly generated. A structure fingerprinting technique of bond characterization matrix is applied to the generated structures, so that identical structures are strictly forbidden. These procedures significantly enhance the diversity of the structures, which is crucial for the efficiency of the global search of structures. For most of the cases, the structure searching simulation for each calculation was stopped after we generated 1000 ~ 1200 structures (e.g., about 20 ~ 30 generations).

Higher precision of structure optimization by VASP was adopted for a number of structures with low enthalpies. The cut-off energy for the expansion of wavefunctions into plane waves is set to 950 eV in all calculations, and the Monkhorst-Pack k-mesh with a maximum spacing is 0.032, which gives total energy well converged within ~ 1 meV/atom. The electron-ion interaction was described by means of projector augmented wave with $5s^2 5p^5$ and $2s^2 2p^5$ electrons as valence for I and F atoms, respectively. Afterwards, the structures with lowest enthalpies were used to investigate the energetic stabilities for IF_x (x = 1/3, 1/2, 2/3, and 1 - 12) compounds by the following formula: $\Delta H_f = [H(IF_x) - xH(I) - yH(F)]/(x + 1)$, where $H(IF_x)$ is the enthalpy of the considered compound, H(I) is the enthalpy of elemental I, and H(F) is the enthalpy of elemental F. DFT calculations on molecular fragments were made using Gaussian 16, revision B.01.[5] Atomic charges have been calculated using quantum theory of atoms-in-molecules (QTAIM).[6]

Supplementary Figures

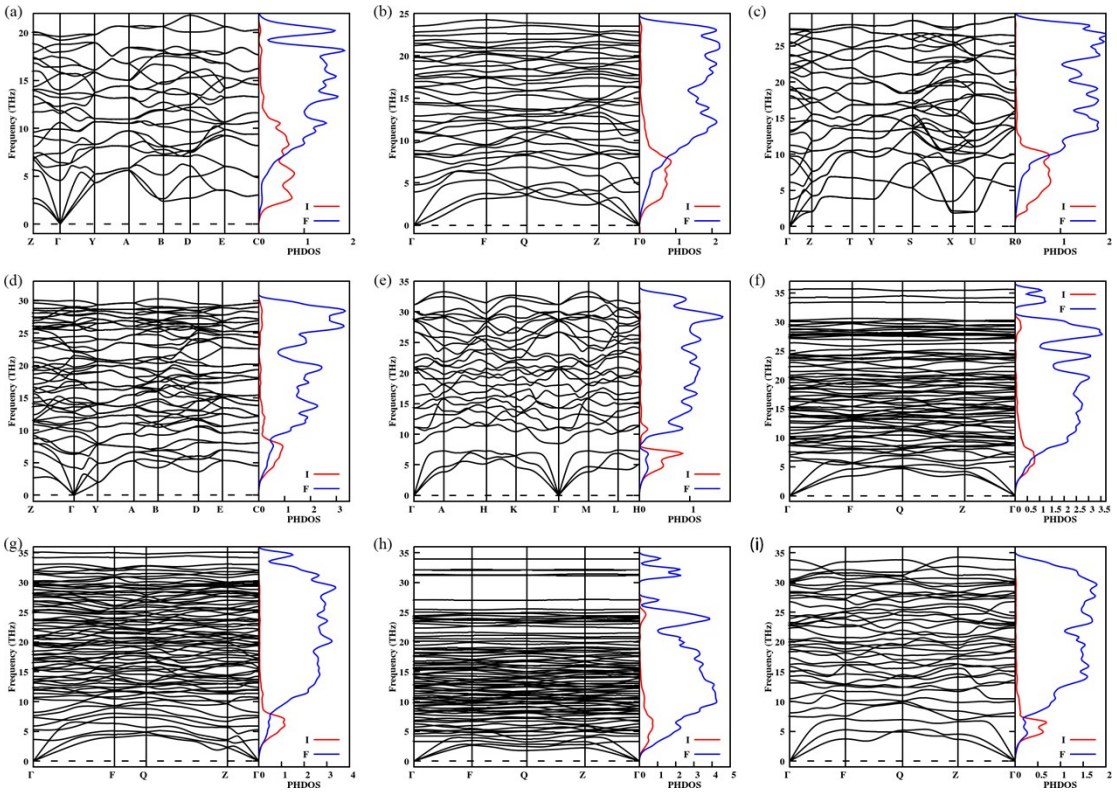

Figure S1. Phonon dispersion curves and phonon density of states (PHDOS) projected on I and F atoms of I-F compounds. (a) IF_3 in $P2_1/m$ structure at 100 GPa. (b-c) IF_5 with P-1 symmetry at 100 GPa and $Pmmm$ symmetry at 200 GPa, respectively. (d) IF_7 in $P2_1/m$ phase at 100 GPa. (e) IF_8 in the R-3 structure at 300 GPa. (f) IF_{10} in P-1 structure at 200 GPa. (g) IF_{11} in P-1 structure at 300 GPa. (h-i) IF_{12} with P-1 symmetry at 100 and 300 GPa, respectively.

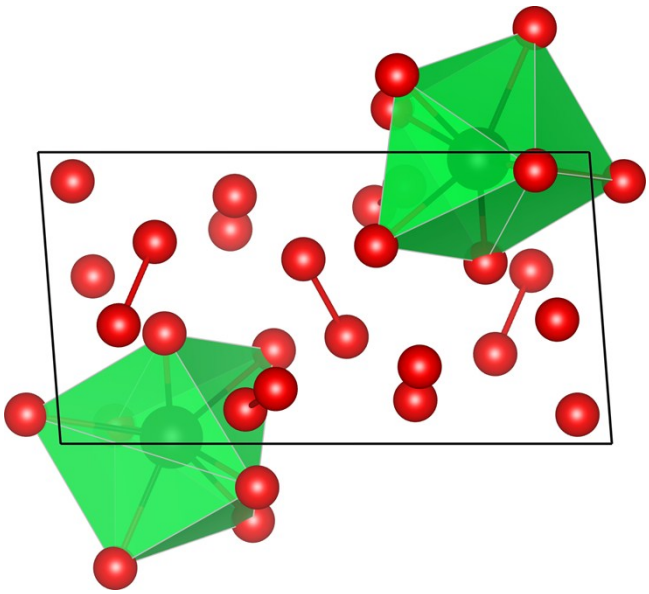

Figure S2. IF_{12} with *P*-1 symmetry at 200 GPa, in which consist of IF_7 and F_2 molecules.

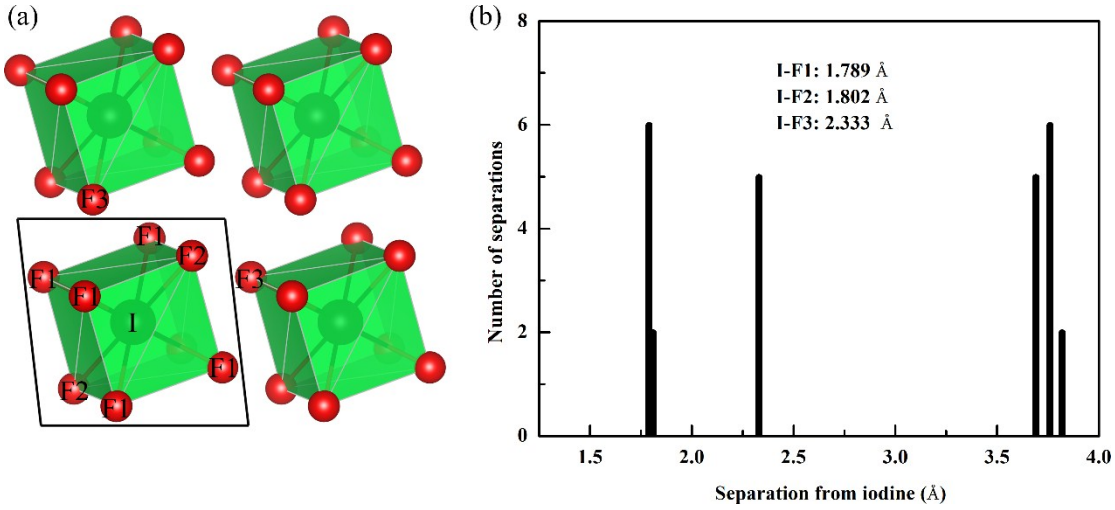

Figure S3. (a) $R\bar{3}$-IF_8 in a 2×2×1 supercell. The primitive cell is drawn with black solid lines. (b) Histograms of I-F separations. Note that the vertical scale, showing the number of nearest neighbors at a given separation.

Why is $Pn\bar{3}n$-structured IF_8 higher in energy compared with $R\bar{3}$-structured IF_8?

A comparison of $Pn\bar{3}n$-structured IF_8 with $R\bar{3}$-structured IF_8 is shown in Figure S4. Partitioning of the total energy clearly reveals that the lower energy of the $R\bar{3}$-phase is due to both the internal energy, *U,* and the pV-term. There is a clear difference between

the two materials discernable in both the COHP-analysis and in the PDOS. For example, I 5d-F 2p interaction within $Pn\bar{3}n$-IF_8 (Figure S4c) shows antibonding states occupied below the Fermi level. This is in contrast to the bonding situation in $R\bar{3}$-IF_8 (Figure 4c), which suggests a key role for the I 5d levels in stabilizing the latter near cubical structure. When comparing the PDOS of I 5d in the two materials, the high energy $Pn\bar{3}n$-phase of IF_8 (Figure S3b) shows unoccupied d_z^2 levels near the Fermi level. These are largely missing in the lower energy $R\bar{3}$-phase (Figure 4d).

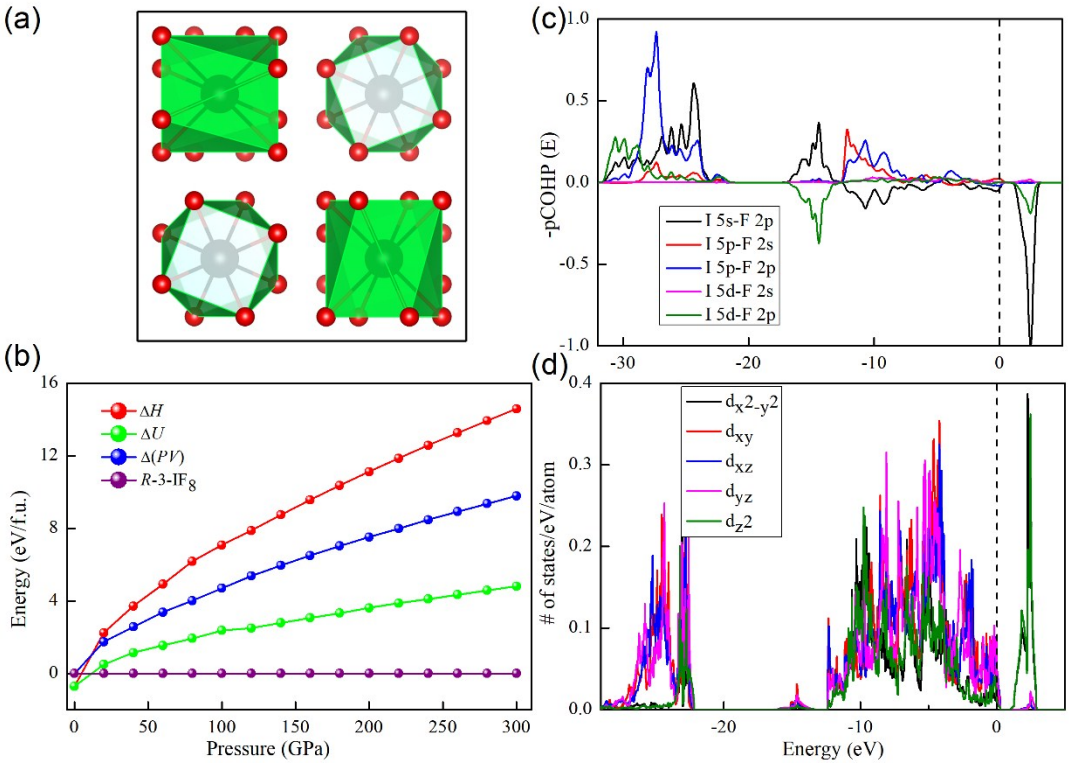

Figure S4. Unstable IF_8 with $Pn\bar{3}n$ symmetry with (a) the square antiprismatic geometry. (b) The calculated change of enthalpy (ΔH), internal energy (ΔU), and $\Delta(PV)$ as a function of pressure of the $Pn\bar{3}n$-IF_8 with respect to $R\bar{3}$-IF_8. (c) Crystal Orbital Hamilton Population (COHP) of $Pn\bar{3}n$-structured IF_8 (d) Partial density of states (PDOS) of I 5d-levels in $Pn\bar{3}n$-structured IF_8 at 300 GPa.

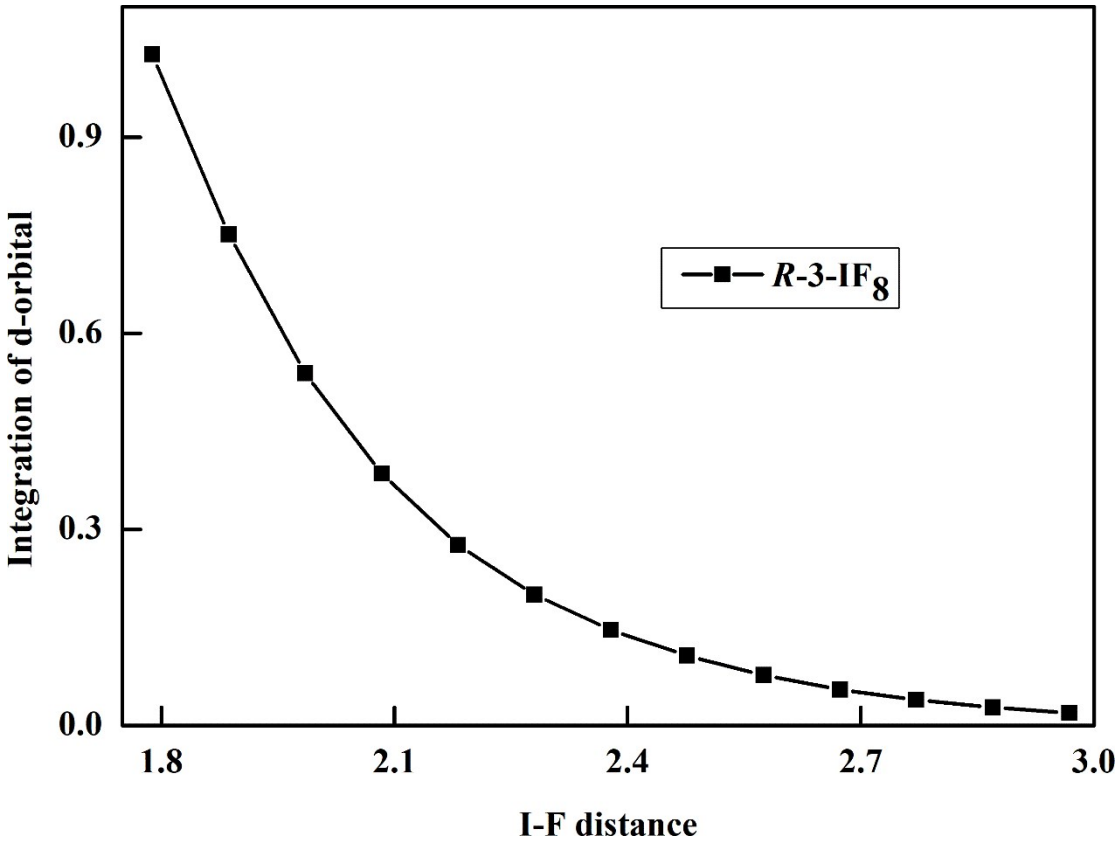

Figure S5. Integration of I 5d in $R\bar{3}$-IF_8 below the Fermi level. Here, we have enlarged the lattice parameters to increase the volume of the F_8 cage in IF_8, and made single point calculations on the frozen geometries. The calculated I d-level PDOS clearly shows the d-participation decreasing (below the Fermi level) as the volume of the F_8 cage increases.

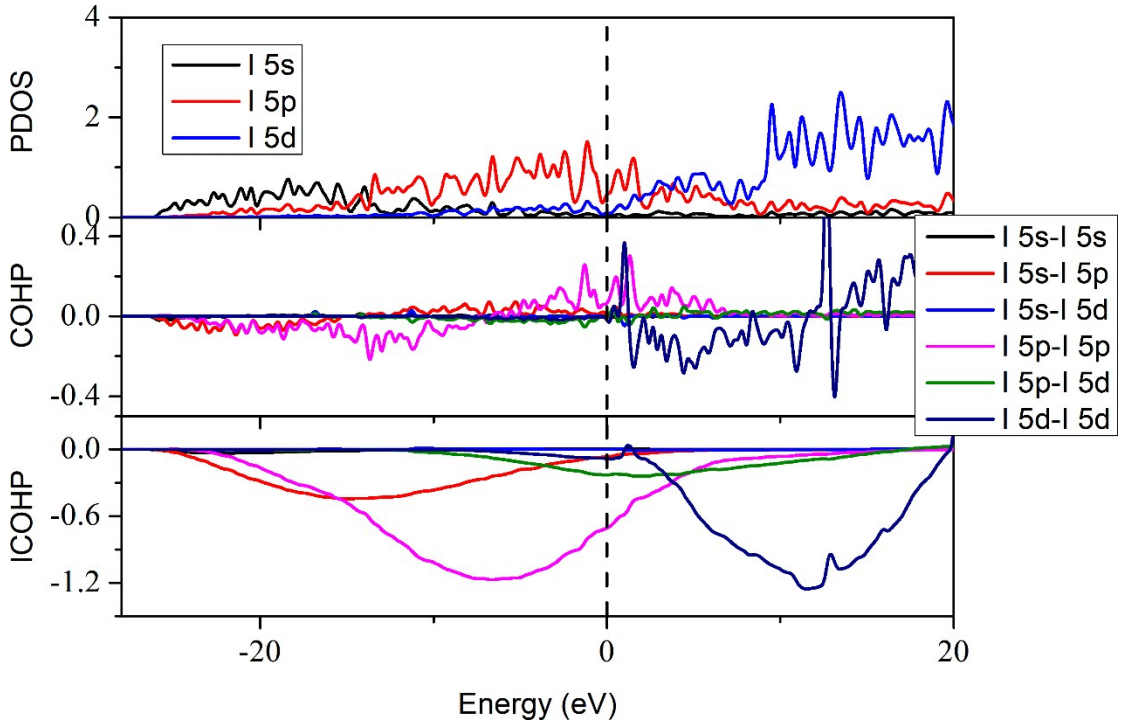

Figure S6. PDOS, COHP and ICOHP of $Fm\bar{3}m$-structured I_2, and the distance of the nearest neighbor I-I bond is 2.63 Å.

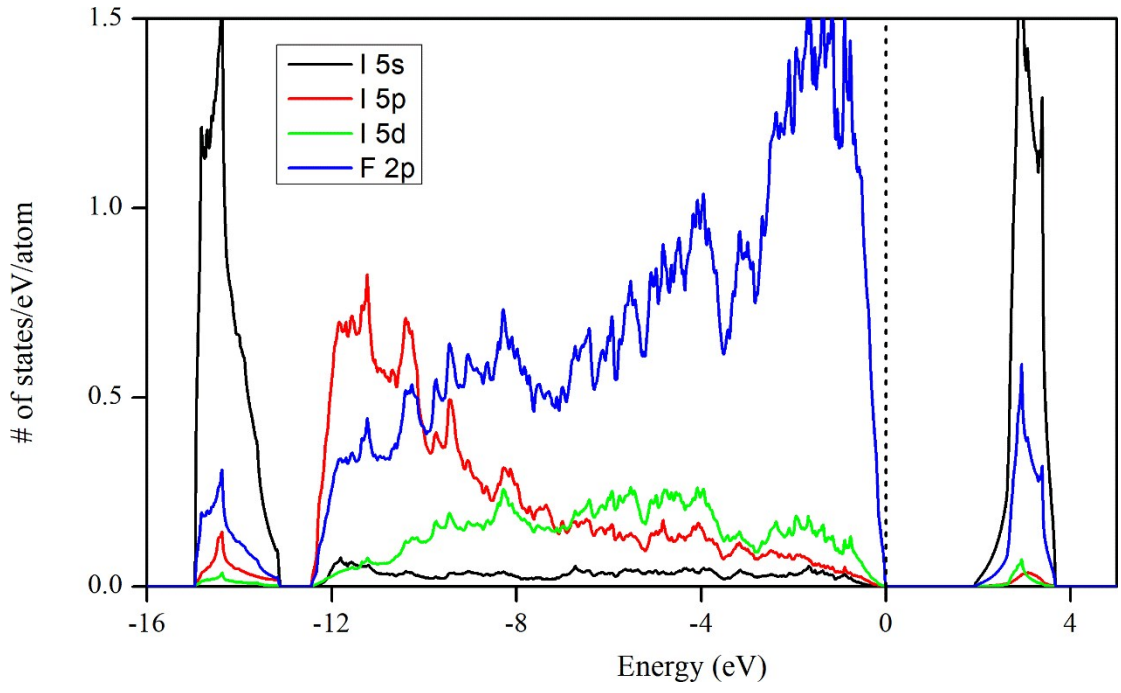

Figure S7. Partial density of states (PDOS) of $P2_1/m$-structured IF_7 at 300 GPa.

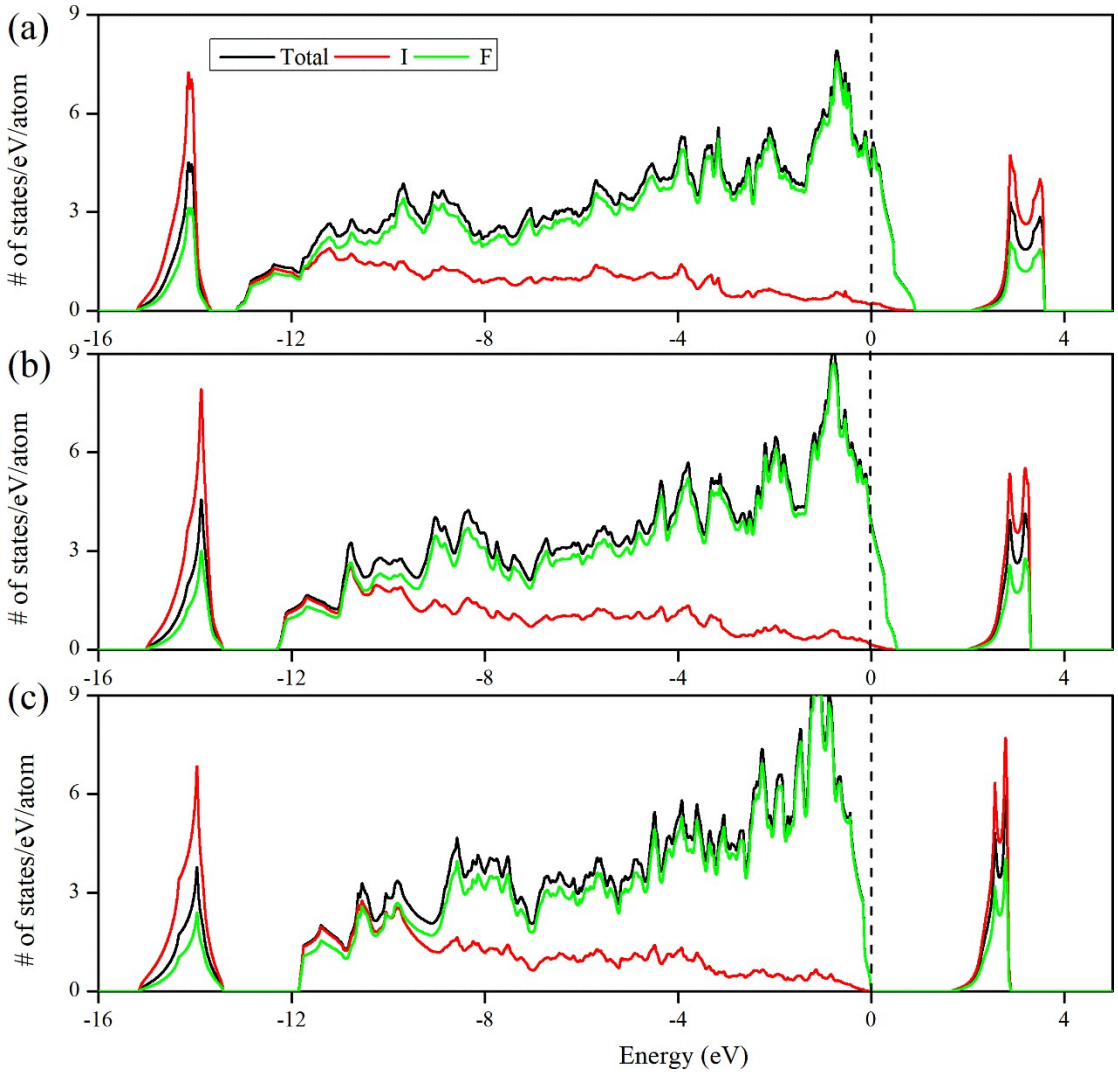

Figure S8. PDOS of I and F in $R\bar{3}$-structured (a) IF_8^+, (b) IF_8 and (c) IF_8^- at 300 GPa.

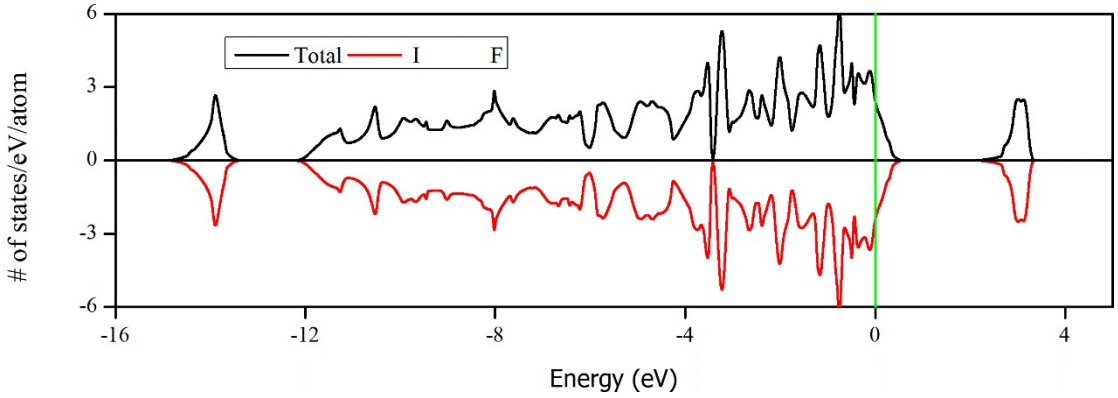

Figure S9. Spin-polarized DOS of $R\bar{3}$-structured IF_8 shows that the material is not magnetic. Magnetic moment of $R\bar{3}$-structured IF_8 is zero.

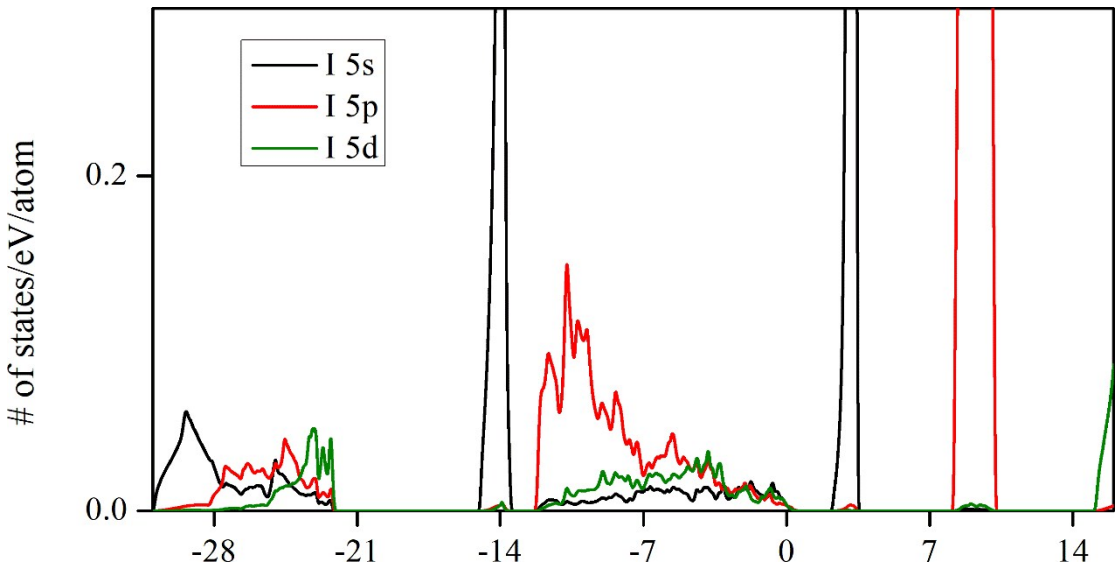

Figure S10. Partial density of states (PDOS) of $R\bar{3}$-structured IF_8 at 300 GPa calculated by WIEN2k.

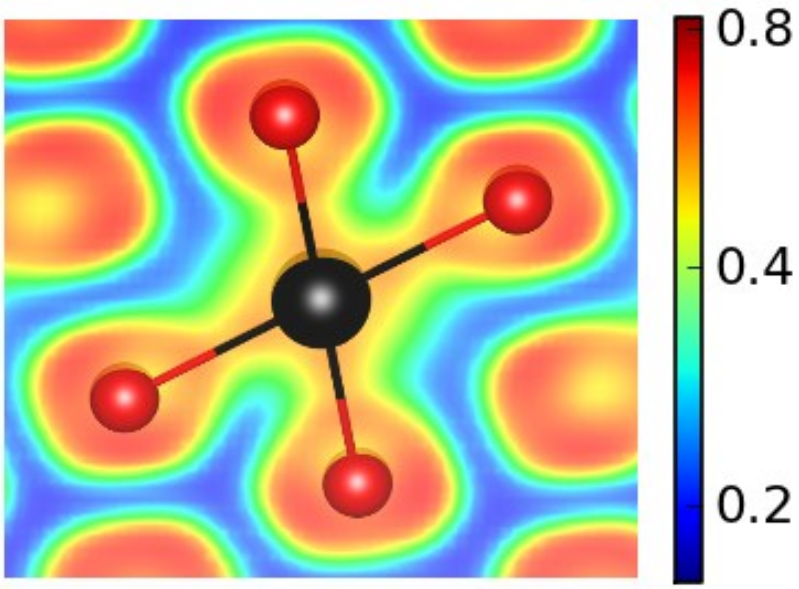

Figure S11. The calculated electron localization functions (ELF) in the F-I-F plane for $R\bar{3}$-structured IF_8 at 300 GPa. ELF ranging from 0.0 (blue) to 0.8 (red) is indicative of a high degree of covalency.

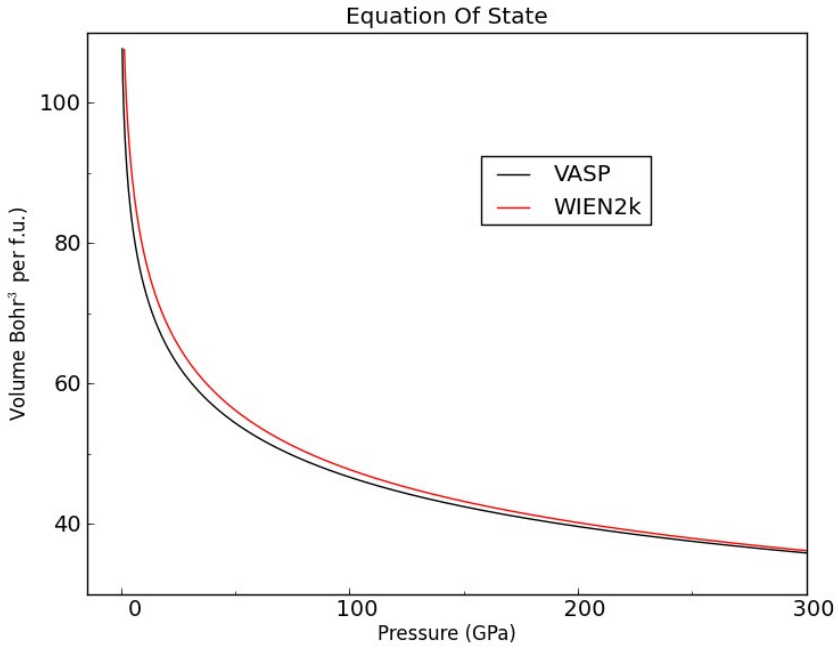

Figure S12. Equation of state for the $R\bar{3}$ phase of IF_8 calculated with pseudopotential-based (VASP) and full-potential (WIEN2k) codes.

Supplementary Tables

Table S1. Decomposition reaction paths and decomposition enthalpies of I-F compounds are assumed as follows. The positive reaction enthalpies indicate these considered phases are metastable.

I-F compounds	Decomposition Reaction path	Decomposition Enthalpy (eV/atom)
	100 GPa	
I_3F	$3\ I_3F \rightarrow 4\ I_2 + IF_3$	0.0391
I_2F	$6\ I_2F \rightarrow 5\ I_2 + 2\ IF_3$	0.0475
I_3F_2	$6\ I_3F_2 \rightarrow 7\ I_2 + 4\ IF_3$	0.0470
IF	$3\ IF \rightarrow I_2 + IF_3$	0.0287
IF_2	$6\ IF_2 \rightarrow I_2 + 4\ IF_3$	0.0149
IF_4	$2\ IF_4 \rightarrow IF_3 + IF_5$	0.0295
IF_6	$2\ IF_6 \rightarrow IF_5 + IF_7$	0.0502
IF_8	$3\ IF_8 \rightarrow 2\ IF_7 + IF_{10}$	0.0400
IF_9	$3\ IF_9 \rightarrow IF_7 + 2\ IF_{10}$	0.0333
IF_{11}	$2\ IF_{11} \rightarrow IF_{10} + IF_{12}$	0.0416
	200 GPa	
I_3F	$5\ I_3F \rightarrow 7\ I_2 + IF_5$	0.0686
I_2F	$10\ I_2F \rightarrow 9\ I_2 + 2\ IF_5$	0.0868
I_3F_2	$10\ I_3F_2 \rightarrow 13\ I_2 + 4\ IF_5$	0.0930

IF	$5\ IF \rightarrow 2\ I_2 + IF_5$	0.1082
IF_2	$10\ IF_2 \rightarrow 3\ I_2 + 4\ IF_5$	0.0304
IF_3	$5\ IF_3 \rightarrow I_2 + 3\ IF_5$	0.0688
IF_4	$10\ IF_4 \rightarrow I_2 + 8\ IF_5$	0.0295
IF_6	$2\ IF_6 \rightarrow IF_5 + IF_7$	0.0842
IF_8	$3\ IF_8 \rightarrow 2\ IF_7 + IF_{10}$	0.0366
IF_9	$3\ IF_9 \rightarrow IF_7 + 2\ IF_{10}$	0.0026
IF_{11}	$2\ IF_{11} \rightarrow IF_{10} + IF_{12}$	0.0074
	300 GPa	
I_3F	$5\ I_3F \rightarrow 7\ I_2 + IF_5$	0.1339
I_2F	$10\ I_2F \rightarrow 9\ I_2 + 2\ IF_5$	0.1648
I_3F_2	$10\ I_3F_2 \rightarrow 13\ I_2 + 4\ IF_5$	0.1722
IF	$5\ IF \rightarrow 2\ I_2 + IF_5$	0.1846
IF_2	$10\ IF_2 \rightarrow 3\ I_2 + 4\ IF_5$	0.1135
IF_3	$5\ IF_3 \rightarrow I_2 + 3\ IF_5$	0.1096
IF_4	$10\ IF_4 \rightarrow I_2 + 8\ IF_5$	0.1158
IF_6	$2\ IF_6 \rightarrow IF_5 + IF_7$	0.0511
IF_9	$3\ IF_9 \rightarrow 2\ IF_8 + IF_{11}$	0.0034
IF_{10}	$3\ IF_{10} \rightarrow IF_8 + 2\ IF_{11}$	0.0214

Table S2. Details structures used for the calculations of decomposition enthalpy.

Phase	Pressure (GPa)	Lattice parameters (Å, °)	Atomic coordinates (fractional)			
IF_3	100	*a* = *3.804*	I (2e)	0.401	0.250	0.170
P*2$_1$/*m		*b* = *3.723*	F(2e)	0.882	0.250	0.364
		c = 4.877	F(2e)	0.969	0.250	0.860
		α = *γ* = 90.000	F(2e)	0.427	0.250	0.623
		β = 99.958				
IF_5	100	*a* = 3.699	I(2i)	0.178	0.647	0.768
***P*-1**		*b* = 3.824	F(2i)	0.380	0.253	0.371
		c = 56.673	F(2i)	0.885	0.250	0.541
		α = 106.193	F(2i)	0.623	0.755	0.956
		β = 90.205	F(2i)	0.618	0.772	0.292
		γ = 103.169	F(2i)	0.108	0.752	0.122
IF_5	200	*a* = 3.393	I(8g)	0.500	0.500	-0.145
Pmmn		*b* = 6.235	F(8g)	0.500	0.166	-0.076
		c = 3.534	F(8g)	0.500	0.666	-0.584
		α = *β* = *γ* = 90.000	F(8g)	0.500	0.000	-0.578
IF_7	100	*a* = 3.854	I(4e)	0.500	0.811	0.250
***C*2/c**		*b* = 8.136	F(8f)	0.789	0.973	0.382
		c = 7.364	F(8f)	0.125	0.148	0.411
		α = *γ* = 90.000	F(8f)	0.334	0.880	0.455
		β = 98.925	F(4e)	0.500	0.780	0.750
IF_7	200	*a* = 4.175	I(2e)	0.676	0.750	0.014
P*2$_1$*m			F(4f)	0.131	0.053	0.768
		b = 6.239	F(4f)	0.359	0.485	0.255
		c = 3.767	F(2e)	0.994	0.750	0.618
		α = 90.000	F(2e)	0.534	0.250	0.523
		β = 78.107	F(2e)	0.744	0.250	0.000
		γ = 90.000				
IF_8	300	*a* = *b* = 5.402	I(3b)	0.000	0.000	0.500
***R*$\bar{3}$**		*c* = 5.626	F(18f)	0.021	0.323	0.604
		α = *β* = 90.000	F(6c)	0.000	0.000	0.179
		γ = 120.000				
IF_{10}	100	*a* = *4.337*	I(2i)	0.974	0.229	0.289
***P*-1**		*b* = 5.632	F(2i)	0.457	0.508	0.093
		c = 6.960	F(2i)	0.707	0.164	0.728
		α = *101.329*	F(2i)	0.978	0.365	0.889
		β = 105.147	F(2i)	0.791	0.865	0.875
		γ = 104.585	F(2i)	0.221	0.111	0.798
			F(2i)	0.354	0.496	0.353
			F(2i)	0.328	0.801	0.949
			F(2i)	0.136	0.471	0.646

			F(2i)	0.775	0.852	0.502
			F(2i)	0.348	0.827	0.588
IF_{11}	300	a = 3.595	I(2i)	0.908	0.398	0.310
***P*-1**		b = 3.690	F(2i)	0.989	0.847	0.912
		c = 9.449	F(2i)	0.795	0.642	0.535
		α = 95.018	F(2i)	0.606	0.423	0.144
		β = 93.275	F(2i)	0.744	0.949	0.219
		γ = 98.520	F(2i)	0.353	0.863	0.570
			F(2i)	0.587	0.104	0.948
			F(2i)	0.918	0.152	0.609
			F(2i)	0.198	0.367	0.986
			F(2i)	0.832	0.342	0.816
			F(2i)	0.704	0.839	0.737
			F(2i)	0.467	0.357	0.647
IF_{12}	100	a = 3.810	I(2i)	0.023	0.273	0.202
***P*-1**		b = 6.944	F(2i)	0.938	0.926	0.900
		c = 7.242	F(2i)	0.594	0.105	0.878
		α = 74.123	F(2i)	0.900	0.608	0.058
		β = 97.915	F(2i)	0.308	0.211	0.801
		γ = 103.937	F(2i)	0.188	0.867	0.398
			F(2i)	0.379	0.498	0.204
			F(2i)	0.574	0.280	0.818
			F(2i)	0.367	0.411	0.534
			F(2i)	0.150	0.609	0.650
			F(2i)	0.882	0.321	0.660
			F(2i)	0.261	0.955	0.662
			F(2i)	0.321	0.171	0.400
IF_{12}	200	a = 3.811	I(1a)	0.000	0.000	0.000
***P*-1**		b = 4.624	F(2i)	0.494	0.954	0.234
		c = 4.727	F(2i)	0.155	0.705	0.914
		α = 68.192	F(2i)	0.610	0.712	0.683
		β = 107.258	F(2i)	0.765	0.488	0.609
		γ = 97.940	F(2i)	0.076	0.853	0.434
			F(2i)	0.289	0.354	0.862

Table S3. Bond length for IF_n ($n > 2$) compound. The I-I bond length in solid is 2.715 at 0 GPa, F-F bond length in molecule F_2 is 1.440 Å at 0 GPa.

Phase	Pressure (GPa)	I-F (Å)	F-F (Å)	I-I (Å)
IF_3-*P*2$_1$/*m*	100	1.909	2.530	4.277
IF_5-*P*-1	100	1.867	2.125	3.583
IF_5-*Pmmm*	200	1.863	2.033	3.393
IF_7-*C*2/*c*	100	1.766	1.957	3.854
IF_7-*P*2$_1$/*m*	200	1.763	1.948	3.459
IF_8-*R*$\bar{3}$	300	1.789	1.894	3.639
IF_{10}-*P*-1	100	1.787	1.433	3.706
IF_{11}-*P*-1	300	1.775	3.595	1.431
IF_{12}-*P*-1(I)	100	1.779	3.810	1.416
IF_{12}-*P*-1(II)	200	1.773	3.811	1.450

Table S4. Integration of I 5d in *R*$\bar{3}$-IF_8 below the Fermi level. Note that the PDOS is calculated by VASP and shown in Figure 4d. The integrated results show slightly more electrons occupying d_z^2 orbital than the other four d orbitals, which may explain the small structural deviation from a perfect cube.

Energy range	Integration of five I d				
-55 to 0 eV	d_z^2	$d_{x^2-y^2}$	d_{xy}	d_{xz}	d_{yz}
	0.27	0.22	0.22	0.15	0.17

References

1. Y. Wang, J. Lv, L. Zhu, Y. Ma, Crystal Structure Prediction via Particle-Swarm Optimization, *Phy. Rew. B*, 2010, **82**, 094116.

2. Y. Wang, J. Lv, L. Zhu, Y. Ma, CALYPSO: A Method for Crystal Structure Prediction, *Comput. Phys. Commun.*, 2012, **183**, 2063-2070.

3. G. Kresse, J. Furthmüller, Efficient Iterative Schemes for Ab Initio Total-Energy Calculations Using a Plane-Wave Basis Set, *Phy. Rew. B*, 1996, **54**, 11169.

4. J. P. Perdew, K. Burke, M. Ernzerhof, Generalized Gradient Approximation Made Simple, *Phys. Rev. Lett.*, 1996, **77**, 3865.

5. Gaussian 16, Revision B.01, M. J. Frisch, G. W. Trucks, H. B.Schlegel, G. E. Scuseria, M. A.Robb, J. R.Cheeseman, G. Scalmani, V. Barone, G. A. Petersson, H. Nakatsuji, X. Li, M. Caricato, A. V. Marenich, J. Bloino, B. G.Janesko, R.Gomperts, B.Mennucci, H. P. Hratchian, J. V. Ortiz, A. F. Izmaylov, J. L. Sonnenberg, D. Williams-Young, F. Ding, F. Lipparini, F. Egidi, J. Goings, B. Peng, A. Petrone, T. Henderson, D. Ranasinghe, V. G. Zakrzewski, J. Gao, N. Rega, G. Zheng, W. Liang, M. Hada, M. Ehara, K. Toyota, R. Fukuda, J. Hasegawa, M. Ishida, T. Nakajima, Y. Honda, O. Kitao, H. Nakai, T. Vreven, K. Throssell, J. A. Montgomery Jr., J. E. Peralta, F. Ogliaro, M. J. Bearpark, J. J. Heyd, E. N. Brothers, K. N. Kudin, V. N. Staroverov, T. A. Keith, R. Kobayashi, J. Normand, K. Raghavachari, A. P. Rendell, J. C. Burant, S. S. Iyengar, J. Tomasi, M. Cossi, J. M. Millam, M. Klene, C. Adamo, R. Cammi, J. W. Ochterski, R. L. Martin, K. Morokuma, O. Farkas, J. B. Foresman, D. J. Fox, Gaussian, Inc., Wallingford CT, 2016.

6. R. F. Bader, A quantum theory of molecular structure and its applications, *Chem. Rev.*, 1991, **91**, 893-928.